Weyl semimetal in a topological insulator multilayer*

Physics 596 Journal Club

Xuefei Guo, Daniel Gysbers, Porter Howland, Zemin Huang

December 7, 2018

University of Illinois, Urbana-Champaign

*A. Burkov and L. Balents. **Weyl semimetal in a topological insulator multilayer**. *Physical Review Letters*, 107(12):127205, 2011.

Outline

Introduction and Motivation

Weyl Semimetals and Dirac's Equation

The Hamiltonian of Dirac's equation is

$$H = \begin{pmatrix} (-i\boldsymbol{\nabla}) \cdot \boldsymbol{\sigma} & M \\ M & -(-i\boldsymbol{\nabla}) \cdot \boldsymbol{\sigma} \end{pmatrix}.$$

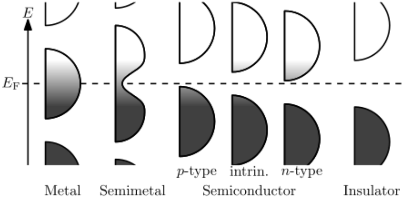

Weyl Semimetals and Dirac's Equation

The Hamiltonian of Dirac's equation is

$$H = \begin{pmatrix} (-i\boldsymbol{\nabla})\cdot\boldsymbol{\sigma} & M \\ M & -(-i\boldsymbol{\nabla})\cdot\boldsymbol{\sigma} \end{pmatrix}.$$

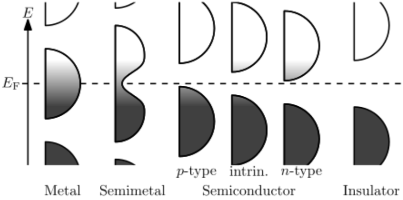

Features:

Weyl Semimetals and Dirac's Equation

The Hamiltonian of Dirac's equation is

$$H = \begin{pmatrix} (-i\boldsymbol{\nabla})\cdot\boldsymbol{\sigma} & M \\ M & -(-i\boldsymbol{\nabla})\cdot\boldsymbol{\sigma} \end{pmatrix}.$$

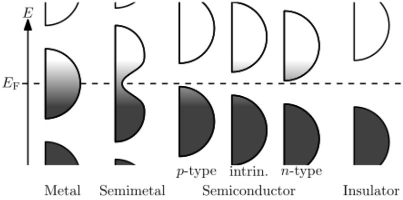

Features:

- four-band massive fermions

Weyl Semimetals and Dirac's Equation

The Hamiltonian of Dirac's equation is

$$H = \begin{pmatrix} (-i\boldsymbol{\nabla}) \cdot \boldsymbol{\sigma} & M \\ M & -(-i\boldsymbol{\nabla}) \cdot \boldsymbol{\sigma} \end{pmatrix}.$$

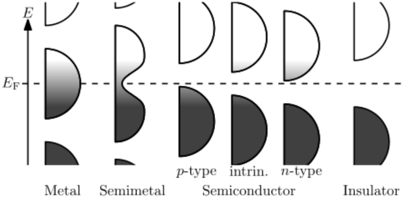

Features:

- four-band massive fermions
- time-reversal symmetry (TR) and parity (or inversion symmetry)

Weyl Semimetals and Dirac's Equation

The Hamiltonian of Dirac's equation is

$$H = \begin{pmatrix} (-i\boldsymbol{\nabla})\cdot\boldsymbol{\sigma} & M \\ M & -(-i\boldsymbol{\nabla})\cdot\boldsymbol{\sigma} \end{pmatrix}.$$

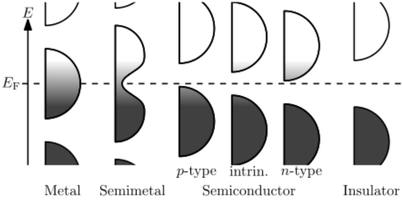

Features:

- four-band massive fermions
- time-reversal symmetry (TR) and parity (or inversion symmetry)
- Lorentz covariant

Weyl Semimetals from Weyl's equation

Weyl's equation (massless Dirac fermions):

$$H = \begin{pmatrix} \overset{(\equiv H_{s=+1})}{(-i\boldsymbol{\nabla}) \cdot \sigma} & \\ & \overset{(\equiv H_{s=-1})}{-(-i\boldsymbol{\nabla}) \cdot \sigma} \end{pmatrix}.$$

Weyl Semimetals from Weyl's equation

Weyl's equation (massless Dirac fermions):

$$H = \begin{pmatrix} \overbrace{(-i\boldsymbol{\nabla}) \cdot \sigma}^{(\equiv H_{s=+1})} & \\ & \overbrace{-(-i\boldsymbol{\nabla}) \cdot \sigma}^{(\equiv H_{s=-1})} \end{pmatrix}.$$

- s for chirality: $+(-)$ for right (left)-handed

Weyl Semimetals from Weyl's equation

Weyl's equation (massless Dirac fermions):

$$H = \begin{pmatrix} \overbrace{(-i\boldsymbol{\nabla})\cdot\sigma}^{(\equiv H_{s=+1})} & \\ & -\overbrace{(-i\boldsymbol{\nabla})\cdot\sigma}^{(\equiv H_{s=-1})} \end{pmatrix}.$$

- s for chirality: $+(-)$ for right (left)-handed
- zero-energy points: Weyl nodes

Weyl Semimetals from Weyl's equation

Weyl's equation (massless Dirac fermions):

$$H = \begin{pmatrix} \overbrace{(-i\boldsymbol{\nabla})}^{(\equiv H_{s=+1})}\cdot\sigma & \\ & -\overbrace{(-i\boldsymbol{\nabla})}^{(\equiv H_{s=-1})}\cdot\sigma \end{pmatrix}.$$

- s for chirality: $+(-)$ for right (left)-handed
- zero-energy points: Weyl nodes
- $H_{s=\pm}$ does not couple with each other: $\partial_\mu j_s^\mu = 0$?!

Weyl Semimetals from Weyl's equation

Weyl's equation (massless Dirac fermions):

$$H = \begin{pmatrix} \overbrace{(-i\boldsymbol{\nabla})}^{(\equiv H_{s=+1})} \cdot \sigma & \\ & -\overbrace{(-i\boldsymbol{\nabla})}^{(\equiv H_{s=-1})} \cdot \sigma \end{pmatrix}.$$

- s for chirality: $+(-)$ for right (left)-handed
- zero-energy points: Weyl nodes
- $H_{s=\pm}$ does not couple with each other: $\partial_\mu j_s^\mu = 0$?!

Weyl Semimetals from Weyl's equation

Weyl's equation (massless Dirac fermions):

$$H = \begin{pmatrix} \overbrace{(-i\boldsymbol{\nabla})\cdot\sigma}^{(\equiv H_{s=+1})} & \\ & -\overbrace{(-i\boldsymbol{\nabla})\cdot\sigma}^{(\equiv H_{s=-1})} \end{pmatrix}.$$

- s for chirality: $+(-)$ for right (left)-handed
- zero-energy points: Weyl nodes
- $H_{s=\pm}$ does not couple with each other: $\partial_\mu j_s^\mu = 0$?!

Breaking TR and inversion symmetry?

Weyl Semimetals from Weyl's equation

Weyl's equation (massless Dirac fermions):

$$H = \begin{pmatrix} \overset{(\equiv H_{s=+1})}{(-i\boldsymbol{\nabla}) \cdot \sigma} & \\ & \overset{(\equiv H_{s=-1})}{-(-i\boldsymbol{\nabla}) \cdot \sigma} \end{pmatrix}.$$

- s for chirality: $+(-)$ for right (left)-handed
- zero-energy points: Weyl nodes
- $H_{s=\pm}$ does not couple with each other: $\partial_\mu j^\mu_s = 0$?!

Breaking TR and inversion symmetry?

$$H_s = (-is\boldsymbol{\nabla} - s\boldsymbol{\lambda}) \cdot \boldsymbol{\sigma} + \lambda_0.$$

Weyl nodes, Weyl semimetals.

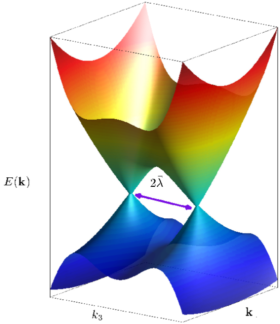

Energy spectrum, Cortijo et al. (2015).

Why are Weyl Semimetals Interesting?

- **Protected by topology**: Berry's curvature, monopole charge . . .

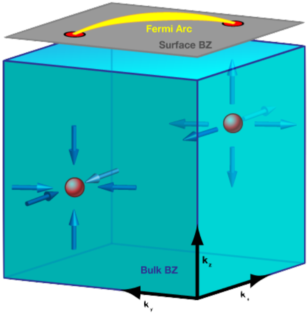

Monopoles in Weyl semimetals and Fermi arcs.[1]

[1]Balents (2011)

Why are Weyl Semimetals Interesting?

- **Protected by topology**: Berry's curvature, monopole charge . . .
- **Novel responses**: the chiral magnetic effect, the anomalous quantum Hall effect . . .

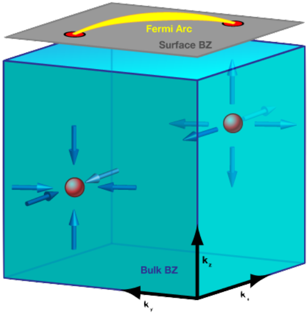

Monopoles in Weyl semimetals and Fermi arcs.[1]

[1] Balents (2011)

Why are Weyl Semimetals Interesting?

- **Protected by topology**: Berry's curvature, monopole charge ...
- **Novel responses**: the chiral magnetic effect, the anomalous quantum Hall effect ...
- **High-energy physics in condensed matters**: chiral anomaly, gravitational anomaly, Riemann-Cartan geometry ...

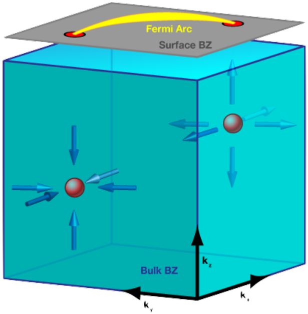

Monopoles in Weyl semimetals and Fermi arcs.[1]

[1] Balents (2011)

Chiral Anomaly $\partial_\mu j_s^\mu \neq 0$ from the Lowest Landau Level

- turn on the magnetic fields: the chiral lowest Landau level

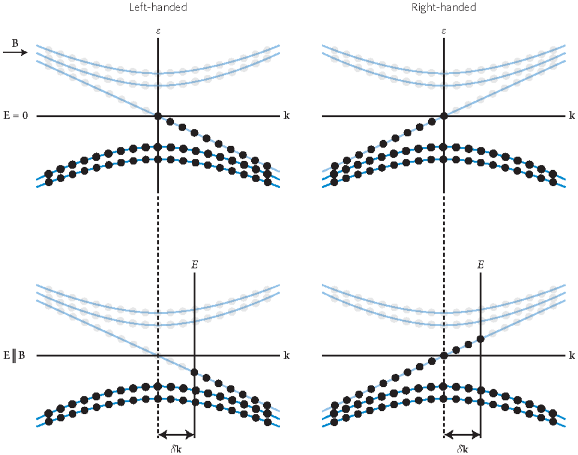

Landau's level of Weyl's equation Burkov (2016)

Chiral Anomaly $\partial_\mu j_s^\mu \neq 0$ from the Lowest Landau Level

- turn on the magnetic fields: the chiral lowest Landau level
- turn on the electric fields

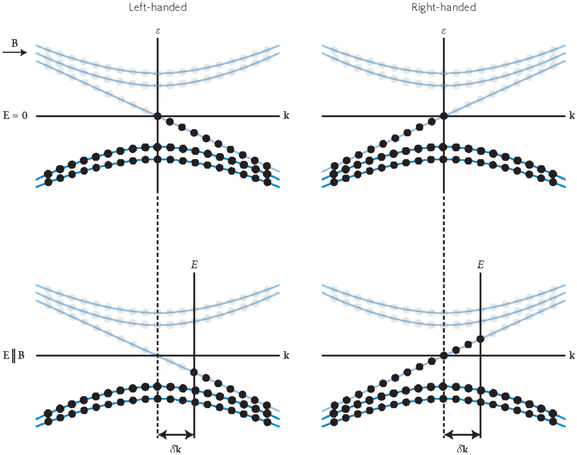

Landau's level of Weyl's equation Burkov (2016)

Chiral Anomaly $\partial_\mu j_s^\mu \neq 0$ from the Lowest Landau Level

- turn on the magnetic fields: the chiral lowest Landau level
- turn on the electric fields
- chiral anomaly: $\partial_\mu j_s^\mu = \frac{s}{4\pi^2} \boldsymbol{E} \cdot \boldsymbol{B}$ s-Weyl fermions are not independent. Anomaly!

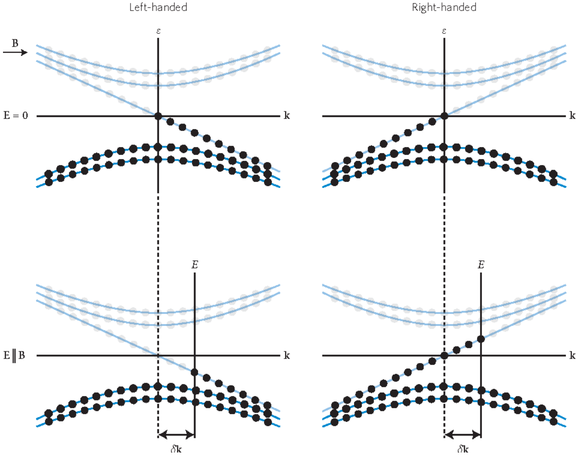

Landau's level of Weyl's equation Burkov (2016)

Chiral Anomaly from Berry's Curvature

- Monopole charge in momentum space: $\boldsymbol{\nabla} \cdot \boldsymbol{\Omega}_s = 2\pi s \delta^3(\boldsymbol{p})$, Ω_s, magnetic field in momentum space for s-Weyl fermions

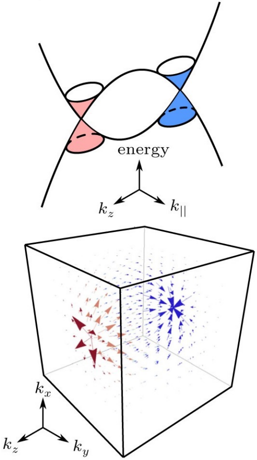

Berry connection in Weyl semimetals (in momentum space).[1]

[1] Lu and Shen (2017)

Chiral Anomaly from Berry's Curvature

- Monopole charge in momentum space: $\boldsymbol{\nabla} \cdot \boldsymbol{\Omega}_s = 2\pi s \delta^3(\boldsymbol{p})$, Ω_s, magnetic field in momentum space for s-Weyl fermions
- Breakdown of Liouville's Theorem due to monopole charge!

$$\frac{\partial D_s}{\partial t} = \underbrace{\{D_s, H\}}_{\text{Poisson Bracket}} + \underbrace{(\boldsymbol{\nabla} \cdot \boldsymbol{\Omega}_s)}_{\text{Monopole}} \boldsymbol{E} \cdot \boldsymbol{B},$$

where D_s is the density of states. Chiral anomaly!

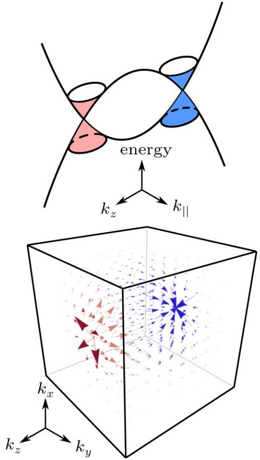

Berry connection in Weyl semimetals (in momentum space).[1]

[1] Lu and Shen (2017)

The Paper

Simple Multilayer Weyl Semimetal Model

- Purpose: Creating a simple Weyl semimetal model

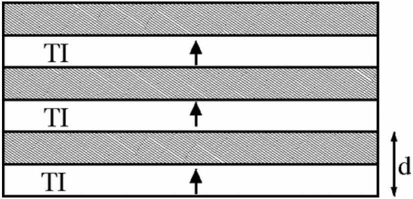

Drawing of proposed multilayer structure. Arrow shows magnetization direction.[1]

[1] Burkov and Balents (2011)

Simple Multilayer Weyl Semimetal Model

- Purpose: Creating a simple Weyl semimetal model
- Alternating layers of a topological insulator (TI) and an ordinary insulator

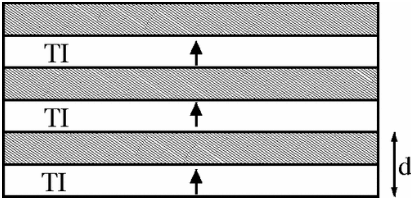

Drawing of proposed multilayer structure. Arrow shows magnetization direction.[1]

[1] Burkov and Balents (2011)

Simple Multilayer Weyl Semimetal Model

- Purpose: Creating a simple Weyl semimetal model
- Alternating layers of a topological insulator (TI) and an ordinary insulator
- Two Weyl fermions at same point in momentum space, topologically unstable

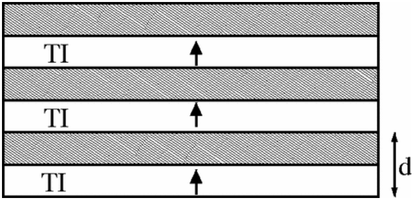

Drawing of proposed multilayer structure. Arrow shows magnetization direction.[1]

[1] Burkov and Balents (2011)

Simple Multilayer Weyl Semimetal Model

- Purpose: Creating a simple Weyl semimetal model
- Alternating layers of a topological insulator (TI) and an ordinary insulator
- Two Weyl fermions at same point in momentum space, topologically unstable
- Add magnetic impurities to each TI layer

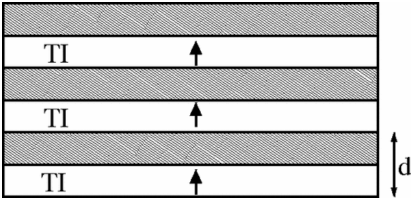

Drawing of proposed multilayer structure. Arrow shows magnetization direction.[1]

[1] Burkov and Balents (2011)

Simple Multilayer Weyl Semimetal Model

- Purpose: Creating a simple Weyl semimetal model
- Alternating layers of a topological insulator (TI) and an ordinary insulator
- Two Weyl fermions at same point in momentum space, topologically unstable
- Add magnetic impurities to each TI layer
- Spin splitting of surface states, separates Dirac nodes

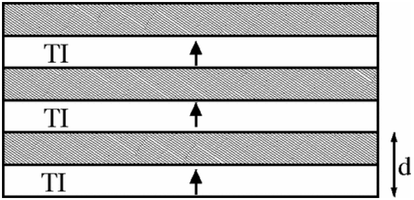

Drawing of proposed multilayer structure. Arrow shows magnetization direction.[1]

[1] Burkov and Balents (2011)

Simple Multilayer Weyl Semimetal Model

- Purpose: Creating a simple Weyl semimetal model
- Alternating layers of a topological insulator (TI) and an ordinary insulator
- Two Weyl fermions at same point in momentum space, topologically unstable
- Add magnetic impurities to each TI layer
- Spin splitting of surface states, separates Dirac nodes
- Stable Weyl semimetal phase

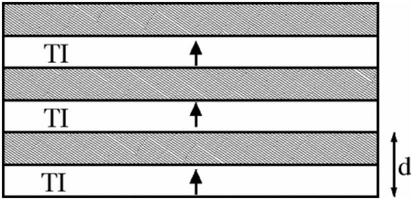

Drawing of proposed multilayer structure. Arrow shows magnetization direction.[1]

[1] Burkov and Balents (2011)

Model Hamiltonian and Phase Diagrams

Model Hamiltonian

The heterostructure Hamiltonian can be written as $(\hbar = 1)$:

$$H = \sum_{\boldsymbol{k}_\perp, i, j} \Big[v_F \tau^z \left(\hat{z} \times \boldsymbol{\sigma} \right) \cdot \boldsymbol{k}_\perp \delta_{i,j} + m\sigma^z \delta_{i,j} + \Delta_S \tau^x \delta_{i,j} + \frac{1}{2} \Delta_D \tau^+ \delta_{j,i+1} + \frac{1}{2} \Delta_D \tau^- \delta_{j,i-1} \Big] c^\dagger_{\boldsymbol{k}_\perp i} c_{\boldsymbol{k}_\perp j}.$$

Model Hamiltonian

The heterostructure Hamiltonian can be written as $(\hbar = 1)$:

$$H = \sum_{\boldsymbol{k}_\perp, i, j} \Big[v_F \tau^z \left(\hat{z} \times \boldsymbol{\sigma} \right) \cdot \boldsymbol{k}_\perp \delta_{i,j} + m \sigma^z \delta_{i,j} + \Delta_S \tau^x \delta_{i,j} + \frac{1}{2} \Delta_D \tau^+ \delta_{j,i+1} + \frac{1}{2} \Delta_D \tau^- \delta_{j,i-1} \Big] c^\dagger_{\boldsymbol{k}_\perp i} c_{\boldsymbol{k}_\perp j}.$$

- The first term describes the two (top and bottom) surface states of an individual TI layer; v_F is the Fermi velocity, $\boldsymbol{\sigma}$ $(\boldsymbol{\tau})$ the triplet of Pauli matrices acting on the real (psuedo-) spin degree of freedom, and i and j label TI layers.

Model Hamiltonian

The heterostructure Hamiltonian can be written as ($\hbar = 1$):

$$H = \sum_{\boldsymbol{k}_\perp, i, j} \left[v_F \tau^z \left(\hat{z} \times \boldsymbol{\sigma}\right) \cdot \boldsymbol{k}_\perp \delta_{i,j} + m\sigma^z \delta_{i,j} + \Delta_S \tau^x \delta_{i,j} \right.$$
$$\left. + \frac{1}{2}\Delta_D \tau^+ \delta_{j,i+1} + \frac{1}{2}\Delta_D \tau^- \delta_{j,i-1} \right] c^\dagger_{\boldsymbol{k}_\perp i} c_{\boldsymbol{k}_\perp j}.$$

- The first term describes the two (top and bottom) surface states of an individual TI layer; v_F is the Fermi velocity, $\boldsymbol{\sigma}$ ($\boldsymbol{\tau}$) the triplet of Pauli matrices acting on the real (psuedo-) spin degree of freedom, and i and j label TI layers.
- The second term describes exchange spin splitting of the surface states.

Model Hamiltonian

The heterostructure Hamiltonian can be written as ($\hbar = 1$):

$$H = \sum_{\boldsymbol{k}_\perp, i, j} \Big[v_F \tau^z \left(\hat{z} \times \boldsymbol{\sigma} \right) \cdot \boldsymbol{k}_\perp \delta_{i,j} + m \sigma^z \delta_{i,j} + \Delta_S \tau^x \delta_{i,j} + \frac{1}{2} \Delta_D \tau^+ \delta_{j,i+1} + \frac{1}{2} \Delta_D \tau^- \delta_{j,i-1} \Big] c^\dagger_{\boldsymbol{k}_\perp i} c_{\boldsymbol{k}_\perp j}.$$

- The first term describes the two (top and bottom) surface states of an individual TI layer; v_F is the Fermi velocity, $\boldsymbol{\sigma}$ ($\boldsymbol{\tau}$) the triplet of Pauli matrices acting on the real (psuedo-) spin degree of freedom, and i and j label TI layers.
- The second term describes exchange spin splitting of the surface states.
- The remaining terms describe tunnelling between top and bottom surfaces within the same TI layer.

Phase Diagrams

$$H = \sum_{\boldsymbol{k}_\perp, i, j} \Big[v_F \tau^z (\hat{z} \times \boldsymbol{\sigma}) \cdot \boldsymbol{k}_\perp \delta_{i,j} + m \sigma^z \delta_{i,j} + \Delta_S \tau^x \delta_{i,j}$$

$$\frac{1}{2} \Delta_D \tau^+ \delta_{j,i+1} + \frac{1}{2} \Delta_D \tau^- \delta_{j,i-1} \Big] c^\dagger_{\boldsymbol{k}_\perp i} c_{\boldsymbol{k}_\perp j}.$$

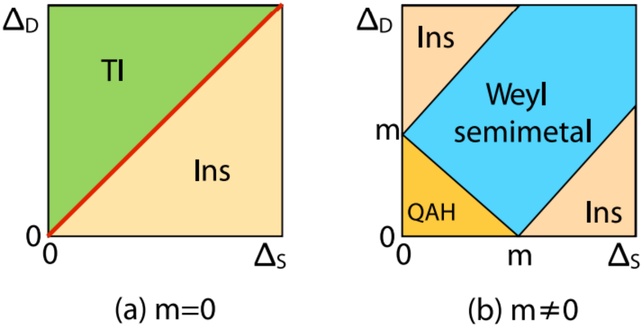

Phase diagrams when m, Δ_S, and Δ_D are treated as tunable parameters.

Phase Diagrams

$$H = \sum_{\mathbf{k}_\perp, i, j} \Big[v_F \tau^z \left(\hat{z} \times \boldsymbol{\sigma}\right) \cdot \mathbf{k}_\perp \delta_{i,j} + \cancel{m\sigma^z \delta_{i,j}} + \Delta_S \tau^x \delta_{i,j}$$

$$\frac{1}{2}\Delta_D \tau^+ \delta_{j,i+1} + \frac{1}{2}\Delta_D \tau^- \delta_{j,i-1} \Big] c^\dagger_{\mathbf{k}_\perp i} c_{\mathbf{k}_\perp j}.$$

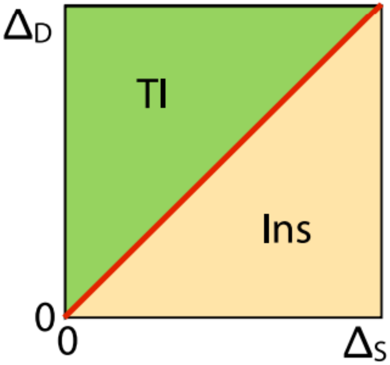

Phase diagram for $m = 0$ (m parameter for spin splitting interaction).

Phase Diagrams

$$H = \sum_{\boldsymbol{k}_\perp, i, j} \Big[v_F \tau^z \left(\hat{z} \times \boldsymbol{\sigma}\right) \cdot \boldsymbol{k}_\perp \delta_{i,j} + \cancel{m\sigma^z \delta_{i,j}} + \Delta_S \tau^x \delta_{i,j}$$

$$\frac{1}{2}\Delta_D \tau^+ \delta_{j,i+1} + \frac{1}{2}\Delta_D \tau^- \delta_{j,i-1} \Big] c^\dagger_{\boldsymbol{k}_\perp i} c_{\boldsymbol{k}_\perp j}.$$

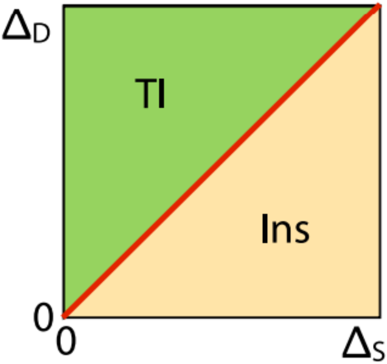

Phase diagram for $m = 0$ (m parameter for spin splitting interaction).

- TI: topological insulator phase.

Phase Diagrams

$$H = \sum_{\mathbf{k}_\perp, i, j} \Big[v_F \tau^z \left(\hat{z} \times \boldsymbol{\sigma} \right) \cdot \mathbf{k}_\perp \delta_{i,j} + \cancel{m \sigma^z \delta_{i,j}} + \Delta_S \tau^x \delta_{i,j}$$

$$\frac{1}{2} \Delta_D \tau^+ \delta_{j,i+1} + \frac{1}{2} \Delta_D \tau^- \delta_{j,i-1} \Big] c^\dagger_{\mathbf{k}_\perp i} c_{\mathbf{k}_\perp j}.$$

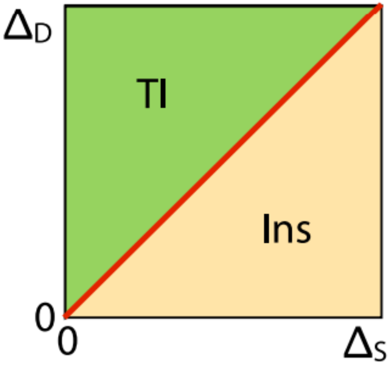

Phase diagram for $m = 0$ (m parameter for spin splitting interaction).

- TI: topological insulator phase.
- Ins: insulator phase.

Phase Diagrams

$$H = \sum_{\boldsymbol{k}_\perp, i, j} \Big[v_F \tau^z \left(\hat{z} \times \boldsymbol{\sigma}\right) \cdot \boldsymbol{k}_\perp \delta_{i,j} + \cancel{m\sigma^z \delta_{i,j}} + \Delta_S \tau^x \delta_{i,j}$$

$$\frac{1}{2}\Delta_D \tau^+ \delta_{j,i+1} + \frac{1}{2}\Delta_D \tau^- \delta_{j,i-1} \Big] c^\dagger_{\boldsymbol{k}_\perp i} c_{\boldsymbol{k}_\perp j}.$$

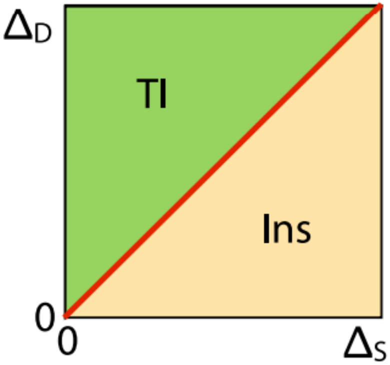

Phase diagram for $m = 0$ (m parameter for spin splitting interaction).

- TI: topological insulator phase.
- Ins: insulator phase.
- Δ_S and Δ_D parameters proportional to the potential barrier in the TI bulk and insulator, respectively.

Phase Diagrams

$$H = \sum_{\mathbf{k}_\perp, i, j} \Big[v_F \tau^z \left(\hat{z} \times \boldsymbol{\sigma}\right) \cdot \mathbf{k}_\perp \delta_{i,j} + m \sigma^z \delta_{i,j} + \Delta_S \tau^x \delta_{i,j}$$

$$\frac{1}{2} \Delta_D \tau^+ \delta_{j,i+1} + \frac{1}{2} \Delta_D \tau^- \delta_{j,i-1} \Big] c^\dagger_{\mathbf{k}_\perp i} c_{\mathbf{k}_\perp j}.$$

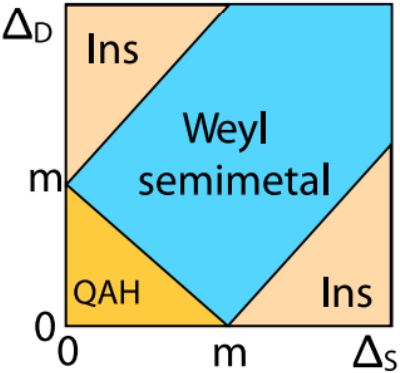

Phase diagram for $m \neq 0$.

- Weyl semimetal phase appears.

Phase Diagrams

$$H = \sum_{\boldsymbol{k}_\perp, i, j} \Big[v_F \tau^z \left(\hat{z} \times \boldsymbol{\sigma}\right) \cdot \boldsymbol{k}_\perp \delta_{i,j} + m\sigma^z \delta_{i,j} + \Delta_S \tau^x \delta_{i,j}$$

$$\frac{1}{2}\Delta_D \tau^+ \delta_{j,i+1} + \frac{1}{2}\Delta_D \tau^- \delta_{j,i-1}\Big] c^\dagger_{\boldsymbol{k}_\perp i} c_{\boldsymbol{k}_\perp j}.$$

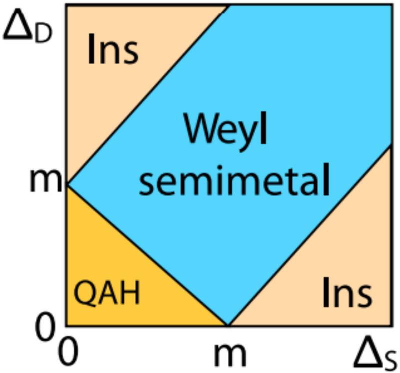

Phase diagram for $m \neq 0$.

- Weyl semimetal phase appears.
- QAH: quantum anomolous hall phase (not important for the main result of the paper).

Experimental Realization?

- Fine tuning of m, Δ_S, and Δ_D

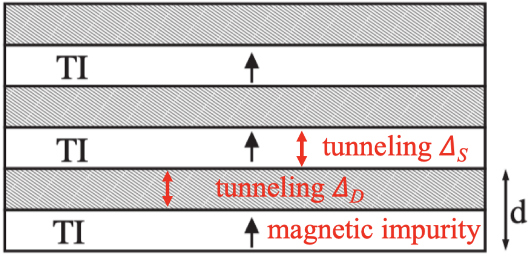

multilayer experimental proposal[1]

Experimental Observations of Weyl Semimetal

- Fine tuning of m, Δ_S, and Δ_D
- suitable magnetic impurity concentration and the magnetic impurity sources

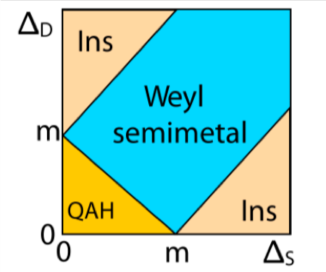

phase diagram of the proposal[1]

[1] Burkov and Balents (2011)

Experimental Observations of Weyl Semimetal

- Fine tuning of m, Δ_S, and Δ_D
- suitable magnetic impurity concentration and the magnetic impurity sources
- Suitable TI and insulator

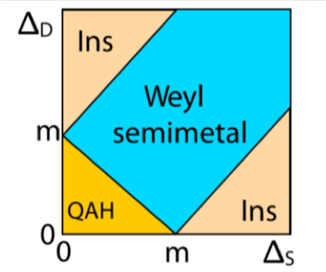

phase diagram of the proposal[1]

[1] Burkov and Balents (2011)

Experimental Observations of Weyl Semimetal

- Fine tuning of m, Δ_S, and Δ_D
- suitable magnetic impurity concentration and the magnetic impurity sources
- Suitable TI and insulator
- Suitable spacing within TI and insulator

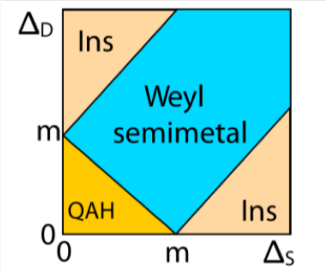

phase diagram of the proposal[1]

[1] Burkov and Balents (2011)

Experimental Observations of Weyl Semimetal

- Fine tuning of m, Δ_S, and Δ_D
- suitable magnetic impurity concentration and the magnetic impurity sources
- Suitable TI and insulator
- Suitable spacing within TI and insulator
- Lack of smoking gun evidence

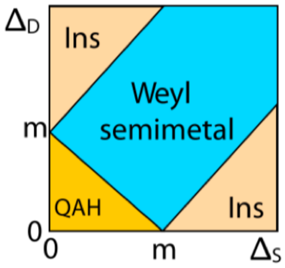

phase diagram of the proposal[1]

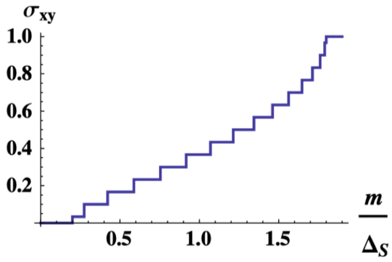

conductivity in units of e^2/hd, where $\Delta_D = 0.8\Delta_S$[1]

[1] Burkov and Balents (2011)

Experimental Observations of Weyl Semimetal

- Until 2015, Dai's group (Weng et al., PRX, 2015) and Hasan's group (Huang et al., Nat. Commun., 2015) proposed TaAs class material

Experimental Observations of Weyl Semimetal

- Until 2015, Dai's group (Weng et al., PRX, 2015) and Hasan's group (Huang et al., Nat. Commun., 2015) proposed TaAs class material
- Surface Fermi arc is the smoking gun

Experimental Observations of Weyl Semimetal

- Until 2015, Dai's group (Weng et al., PRX, 2015) and Hasan's group (Huang et al., Nat. Commun., 2015) proposed TaAs class material
- Surface Fermi arc is the smoking gun
- Angle-Resolved Photoemission Spectroscopy

$$E_{\mathrm{kin}} = h\nu - \phi - |E_B|$$
$$p_{\parallel} = \hbar k_{\parallel} = \sqrt{2mE_{\mathrm{kin}}}\sin\theta$$

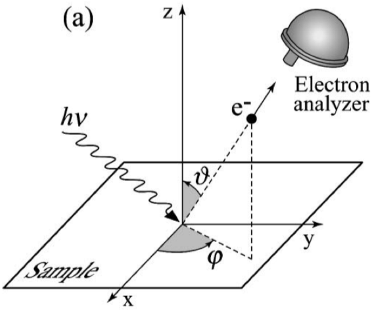

ARPES geometry (Damascelli et al., RMP, 2003)

Experimental Observations of Weyl Semimetal

Ding's group (Lv et al., Nat. Phys. 2015; Lv et al., PRX, 2015): TaAs

Hasan's group (Xu et al., Science, 2015): TaAs

Soljai's group (Lu et al., Science, 2015): photonic crystal

- 12 pairs of Weyl points

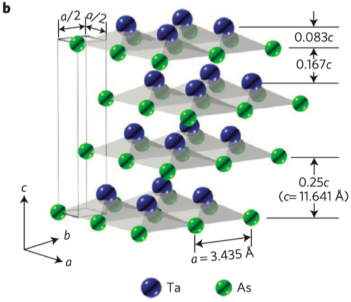

TaAs structure[1]

Experimental Observations of Weyl Semimetal

Ding's group (Lv et al., Nat. Phys. 2015; Lv et al., PRX, 2015): TaAs
Hasan's group (Xu et al., Science, 2015): TaAs
Soljai's group (Lu et al., Science, 2015): photonic crystal

- 12 pairs of Weyl points
- Extended Fermi-arc

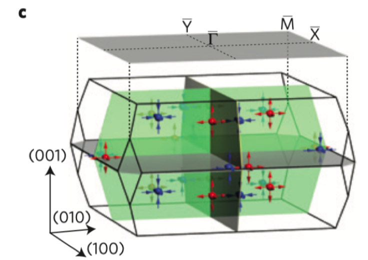

TaAs Brillouin zone and Weyl points[1]

[1] Yang et al. (2015)

Experimental Observations of Weyl Semimetal

Ding's group (Lv et al., Nat. Phys. 2015; Lv et al., PRX, 2015): TaAs
Hasan's group (Xu et al., Science, 2015): TaAs
Soljai's group (Lu et al., Science, 2015): photonic crystal

- 12 pairs of Weyl points
- Extended Fermi-arc

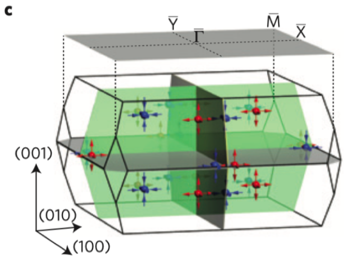

TaAs Brillouin zone and Weyl points[1]

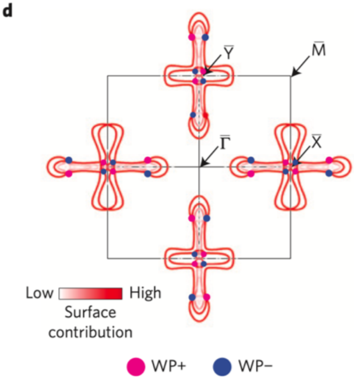

Fermi arc and Weyl nodes from ab initio calculation[1]

[1] Yang et al. (2015)

Excellent agreement between arpes measurement and ab initio calculations

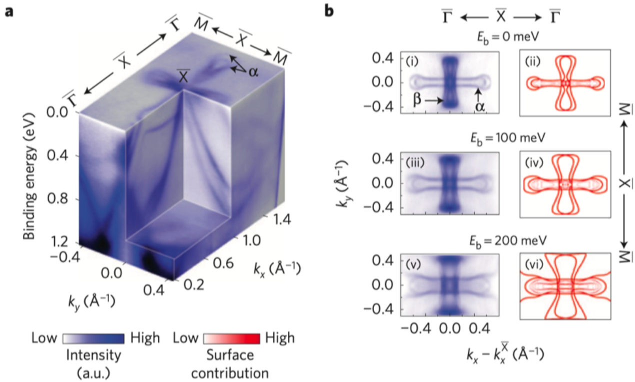

ARPES spectra and ab initio calculation[1]

Experimental Observations of Weyl Semimetal

Excellent agreement between arpes measurement and ab initio calculations

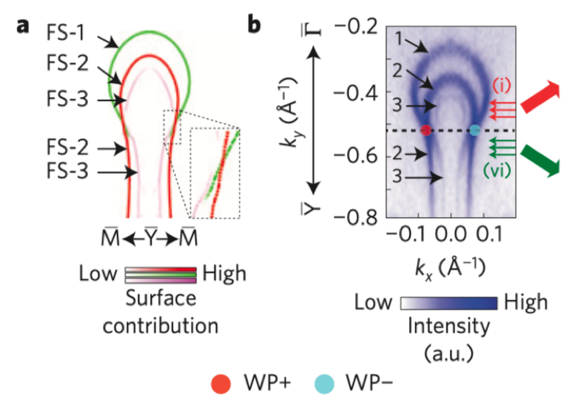

Fermi arc: ab initio (left), and experiment (right)[1]

[1] Yang et al. (2015)

Conclusion and Comments

Citations

- High Impact Paper

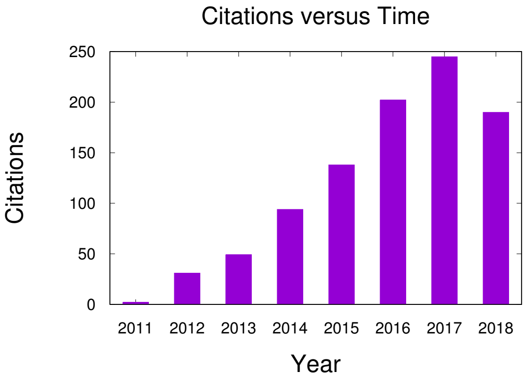

Plot of citations over time from Web of Science data.

Citations

- High Impact Paper
- Physics and Material Science to Geology and Biochemistry

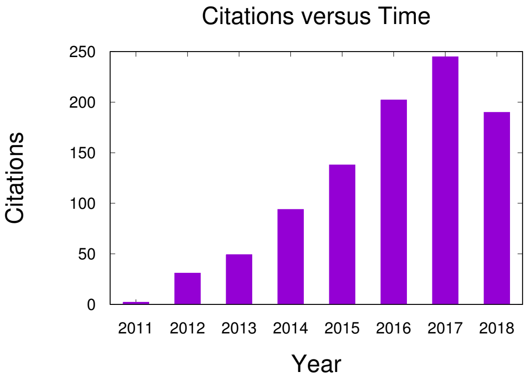

Plot of citations over time from Web of Science data.

Conclusion and Comments

- Simple realization of 3D Weyl semimetal phase

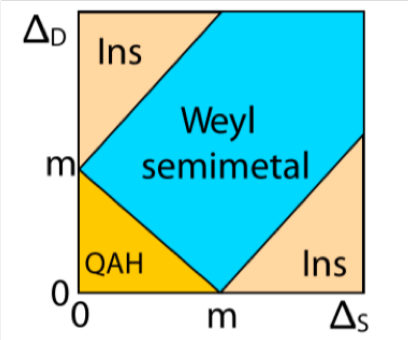

Phase diagram showing Weyl semimetal phase. This is with magnetic doping.[1]

[1] Burkov and Balents (2011)

Conclusion and Comments

- Simple realization of 3D Weyl semimetal phase
- Only two Dirac nodes, simplest possible

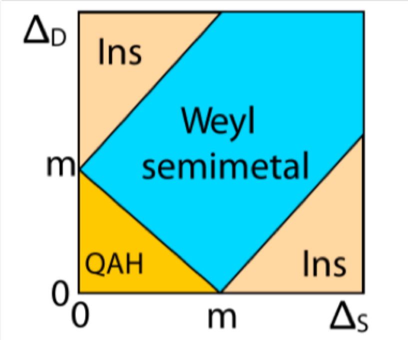

Phase diagram showing Weyl semimetal phase. This is with magnetic doping.[1]

[1] Burkov and Balents (2011)

Conclusion and Comments

- Simple realization of 3D Weyl semimetal phase
- Only two Dirac nodes, simplest possible
- Topologically stable edge states

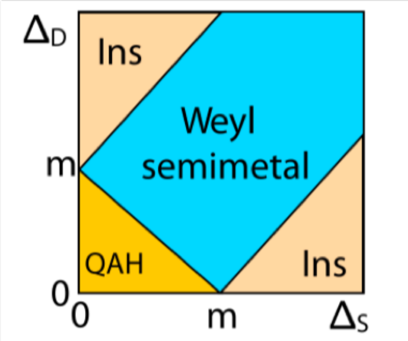

Phase diagram showing Weyl semimetal phase. This is with magnetic doping.[1]

[1] Burkov and Balents (2011)

The Good/Bad

Good

- Good introduction and motivation for the research.

The Good/Bad

Good

- Good introduction and motivation for the research.
- Well laid out explanation with good flow.

The Good/Bad

Good

- Good introduction and motivation for the research.
- Well laid out explanation with good flow.
- Provides a physical picture to understand Weyl semimetals.

The Good/Bad

Good

- Good introduction and motivation for the research.
- Well laid out explanation with good flow.
- Provides a physical picture to understand Weyl semimetals.

The Good/Bad

Good

- Good introduction and motivation for the research.
- Well laid out explanation with good flow.
- Provides a physical picture to understand Weyl semimetals.

Bad

- The internal degree of freedom in each layer is not considered.

The Good/Bad

Good

- Good introduction and motivation for the research.
- Well laid out explanation with good flow.
- Provides a physical picture to understand Weyl semimetals.

Bad

- The internal degree of freedom in each layer is not considered.
- Not great at defining some of the parameters used.

The Good/Bad

Good

- Good introduction and motivation for the research.
- Well laid out explanation with good flow.
- Provides a physical picture to understand Weyl semimetals.

Bad

- The internal degree of freedom in each layer is not considered.
- Not great at defining some of the parameters used.
- Fine tuning of parameters make experiments challenging to realize Weyl semimetal phases.

References

L. Balents. Weyl electrons kiss. *Physics*, 4:36, 2011.

A. Burkov. Topological semimetals. *Nature materials*, 15(11):1145, 2016.

A. Burkov and L. Balents. Weyl semimetal in a topological insulator multilayer. *Physical Review Letters*, 107(12):127205, 2011.

A. Cortijo, Y. Ferreirós, K. Landsteiner, and M. A. Vozmediano. Hall viscosity from elastic gauge fields in dirac crystals. *arXiv preprint arXiv:1506.05136*, 2015.

H.-Z. Lu and S.-Q. Shen. Quantum transport in topological semimetals under magnetic fields. *Frontiers of Physics*, 12(3):127201, 2017.

T. McCormick, I. Kimchi, and N. Trivedi. Minimal models for topological weyl semimetals. *Physical Review B*, 95(07):075133, 2017.

References ii

L. Yang, Z. Liu, Y. Sun, H. Peng, H. Yang, T. Zhang, B. Zhou, Y. Zhang, Y. Guo, M. Rahn, et al. Weyl semimetal phase in the non-centrosymmetric compound taas. *Nature physics*, 11(9):728, 2015.

Experimental Observations So Far

Material	Symmetry Broken	Pairs of Weyl Nodes
TaAs, TaP, NbAs, NbP	Inversion	12
$MoTe_2$	Inversion	4
WTe_2	Inversion	4
LaAlGe	Inversion	20
Ta_3S_2	Inversion	4

Experimental Weyl Semimetals.McCormick et al. (2017)